NPG Asia Materials (2013) 5, e39; doi:10.1038/am.2013.3

www.nature.com/am

ORIGINAL ARTICLE

Highly luminescent silver nanoclusters with tunable emissions: cyclic reduction–decomposition synthesis and antimicrobial properties

Xun Yuan[1], Magdiel Inggrid Setyawati[1], Audrey Shu Tan[1], Choon Nam Ong[2], David Tai Leong[1] and Jianping Xie[1]

This paper reports a facile aqueous-based synthesis method for highly luminescent Ag nanoclusters (NCs) with tunable emissions. The key strategy was to use a reduction–decomposition–reduction cycle to modify the Ag NC intermediates that were further subjected to size/structure focusing. The as-modified Ag NC intermediates were more robust in water against the subsequent etching by thiol ligands, making a mild size-/structure-focusing environment possible, which produced highly luminescent Ag NCs with a well-defined size and structure. Ag NCs with intense red and green emission were successfully synthesized by this method. These Ag NCs possessed a well-defined size and structure ($Ag_{16}(SG)_9$ and $Ag_9(SG)_6$), and exhibited excellent stability in the aqueous phase. Our highly luminescent Ag NCs also possessed superior antimicrobial properties against the multidrug-resistant bacteria *Pseudomonas aeruginosa*, via generating a high concentration of intracellular reactive oxygen species.
NPG Asia Materials (2013) **5,** e39; doi:10.1038/am.2013.3; published online 8 February 2013

Keywords: antimicrobial; biomedical applications; luminescence; silver nanoclusters; thiol ligands

INTRODUCTION

Ultrasmall noble metal nanoclusters (NCs), typically composed of several to a hundred metal atoms, present unique physical and chemical properties between single atoms and large nanocrystals (>2 nm).[1–4] Owing to the strong quantum size confinement in this size range (< 2 nm), NCs possess discrete and size-tunable electronic transitions and display unique molecule-like properties, such as quantized charging and luminescence.[5–12] Strong luminescence is one of the most attractive features of these NCs owing to their ultrafine size, good photostability and low toxicity;[13] some of these properties may not be realized by other luminophores, such as organic dyes (for example, photostability concerns) and semiconductor quantum dots (for example, relatively large size and toxicity concerns).[2,8,9,14,15] Recent studies have shown that luminescent Au and Ag NCs are promising optical probes for bioimaging and biosensing applications.[4,16–20] This finding has led to the development of various methods for the synthesis of highly luminescent Au and Ag NCs.[2,21] On the other hand, insofar as nanostructured Ag-based materials are concerned, they are finding an increasing usage for antimicrobial applications owing to the unique chemistry of Ag interfacing with microorganisms.[22–24] Although there is a large volume of work exploring the potential use of large Ag nanocrystals (>2 nm) as antimicrobials,[25–30] there are no published reports describing the antimicrobial activity of ultrasmall Ag NCs (<2 nm), which could have scaling effects in biological systems that differ from those of their larger counterparts. It is therefore of paramount interest to investigate the potential antimicrobial property of ultrasmall Ag NCs and gain a better understanding of its mechanism. Further, this research may trigger a heightened interest in the synthesis of high-quality luminescent Ag NCs in the aqueous phase.

While good protocols for the synthesis of highly luminescent Au NCs are currently being developed,[6,7,16,31–36] the same cannot be said about the synthesis of luminescent Ag NCs, which were recently discovered. We can broadly classify luminescent Ag NCs that have been successfully synthesized into two types: (1) macromolecule-protected luminescent Ag NCs (for example, polymers,[37–39] dendrimers,[40] DNA[41–43] and proteins[44,45]) and (2) thiol-protected luminescent Ag NCs.[46–52] Among the luminescent Ag NCs, thiol-protected Ag NCs are more attractive for biomedical applications, especially for subcellular imaging, because of their ultrasmall hydrodynamic diameters (<3 nm), facile post-functionalization and good stability. Thiol-protected Ag NCs are generally synthesized by the etching or decomposition method by making use of the unique

[1]Department of Chemical and Biomolecular Engineering, National University of Singapore, Singapore and [2]NUS Environmental Research Institute, National University of Singapore, Singapore
Correspondence: Professor DT Leong or Professor J Xie, Department of Chemical and Biomolecular Engineering, National University of Singapore, 4 Engineering Drive 4, #03-18, 117576, Singapore.
E-mail: cheltwd@nus.edu.sg or chexiej@nus.edu.sg
Received 13 August 2012; revised 7 December 2012; accepted 11 December 2012

thiol–Ag interaction, where large-sized non-luminescent nanocrystals or NCs are etched by thiol ligands to smaller-sized luminescent NCs with a well-defined structure.[47–49,51] Several successful attempts have been recently reported for the generation of luminescent Ag NCs at the organic-water interface or inside the organic phase.[47–49,53] This organic phase synthesis greatly limits its applicability in biomedical settings. The synthesis of luminescent Ag NCs directly in the aqueous phase would therefore expand the bio-usability of Ag NCs. The key challenge faced by the aqueous synthetic route for luminescent Ag NCs is the fast etching kinetics, where an uncontrollable etching process in water quickly degrades Ag NCs by excess thiol ligands into thiolate–Ag^I complexes, which do not show any visible luminescence.[48] Therefore, we predicted that if the etching or size-/structure-focusing kinetics of Ag NCs in water can be slowed, we might be able to synthesize luminescent Ag NCs in the aqueous phase. We then hypothesized that a rational modification of Ag NC intermediates before the etching (or size-/structure-focusing) step could decrease the etching kinetics, favoring the formation of highly luminescent Ag NCs with a well-defined size and structure in water.

Herein, we present a novel synthesis strategy to produce highly luminescent Ag NCs with tunable emissions in the aqueous phase. We took advantage of the unique thiol–Ag interaction to create a reduction–decomposition–reduction cycle (or a cyclic reduction–decomposition route) to modify Ag NC intermediates in water, which were subsequently subjected to a final size-/structure-focusing process. Non-luminescent Ag NC intermediates in a distinct size range were prepared by this cyclic reduction–decomposition method. These modified Ag NC intermediates were found to be more robust against the subsequent etching by thiol ligands in water, creating a relatively mild size-/structure-focusing environment, which can finally transform the Ag NC intermediates into highly luminescent NCs with a well-defined size and structure. Strongly red- and green-emitting Ag NCs (r-Ag NCs and g-Ag NCs) in the aqueous phase were easily produced by this method. The as-synthesized r-Ag NCs and g-Ag NCs definitively contained 16 and 9 Ag atoms, respectively, and displayed superior stability in the aqueous phase. As Ag nanocrystals of larger size are well-documented to be antimicrobial, we hypothesized that ultrasmall Ag NCs will have even higher antimicrobial activity owing to their well-defined structure and high surface area to volume ratio. As expected, the as-synthesized r-Ag NCs demonstrated a unique antimicrobial property against multidrug-resistant bacteria (for example, *P. aeruginosa*), based on its capability of generating the intracellular reactive oxygen species (ROS). Presented below are the details of this investigation.

EXPERIMENTAL PROCEDURE

Materials

Ultrapure Millipore water (18.2 MΩ) was used as the universal solvent unless otherwise indicated. All glassware was washed with aqua regia and rinsed with ethanol and ultrapure water. The following were used as received: sodium borohydride ($NaBH_4$), L-glutathione reduced (GSH), sodium chloride (NaCl), chlorampenicol, rhodamine B, 2,5-dihydroxybenzoic acid (DHB) and 2′,7′-dichlorofluorescein-diacetate (DCF-DA dye) from Sigma-Aldrich (St Louis, MO, USA); sodium hydroxide (NaOH) and silver nitrate ($AgNO_3$) from Merck (Darmstadt, Germany); Bacto tryptone, yeast extract and Bacto agar from BD Difco (Sparks, MD, USA).

Synthesis of r-Ag NCs and g-Ag NCs in water

Aqueous solutions of $AgNO_3$ (20 mM) and GSH (50 mM) were prepared with ultrapure water. An aqueous solution of $NaBH_4$ (112 mM) was freshly prepared by dissolving 43 mg of $NaBH_4$ in 2 ml of 1 M NaOH solution, followed by the addition of 8 ml of ultrapure water. The addition of a certain amount of NaOH to the $NaBH_4$ solution was used to improve the stability of borohydride ions against hydrolysis. In a typical experiment to synthesize r-Ag NCs or g-Ag NCs, aqueous solutions of $AgNO_3$ (125 μl, 20 mM) and GSH (150 μl, 50 mM) were first mixed in water (4.85 ml) under vigorous stirring to form thiolate–Ag^I complexes, followed by the addition of an aqueous solution of $NaBH_4$ (50 μl, 112 mM). A deep-red solution of Ag NCs (~5 ml) was collected after 5 min. This Ag NC solution was then incubated at room temperature for ~3 h, and the deep-red solution gradually decomposed into a colorless solution, leading to the formation of thiolate–Ag^I complexes. Subsequently, a certain amount of 112 mM $NaBH_4$ (50 μl for the synthesis of r-Ag NCs or 250 μl for g-Ag NCs) was introduced into this colorless solution under vigorous stirring, leading to the formation of a light-brown Ag NC solution after 15 min. Without stirring, this light-brown Ag NC solution was incubated at room temperature for a certain period of time (8 h for r-Ag NCs and 48 h for g-Ag NCs). A strong red or green emission was then observed in the aqueous phase. The r-Ag NCs or g-Ag NCs were collected without purification and stored at 4 °C for further characterization.

The instrumentation used in this study and the corresponding detailed experimental procedures for the cell culture, the agar diffusion assay, the reduction of cell growth and the measurement of ROS are described in the Supporting Information.

RESULTS AND DISCUSSION

Synthesis of highly luminescent Ag NCs *via* a cyclic reduction–decomposition process

To demonstrate our designed protocol for highly luminescent thiol-protected Ag NCs in water, a natural tripeptide, glutathione (GSH), was selected as our model thiol ligand. Our protocol involved two stages (Scheme 1): (1) the preparation of modified Ag NC intermediates *via* a cyclic reduction–decomposition route and (2) etching (size-/structure-focusing) of the as-modified Ag NC intermediates to generate highly luminescent Ag NCs. The first stage was to use a reduction–decomposition–reduction cycle to produce modified Ag NC intermediates. Thiolate–Ag^I complexes (hereafter referred to as type-I complexes) were prepared by simply mixing aqueous solutions of silver nitrate ($AgNO_3$) and thiol ligands (GSH). The type-I complexes then underwent a reduction–decomposition–reduction cycle (Scheme 1, Step A–C in Stage I) to prepare the modified Ag NC intermediates.

Scheme 1 can be described by the following three steps. Step A—the reduction of the type-I complexes to form Ag NCs (hereafter referred to as original Ag NC intermediates). The introduction of a certain amount of strong reducing agent, $NaBH_4$, into the type-I complex solution quickly reduced the complexes to form Ag NCs (within 5 min), which displayed a deep-red color in solution under normal light. Step B—the decomposition of the original Ag NC intermediates to form thiolate–Ag^I complexes (hereafter referred to as type-II complexes). The original Ag NC intermediates were unstable in water and degraded rather rapidly in the aqueous phase, as evidenced by the diminishing of the deep-red color in the solution to colorless in 3 h. This color change was owing to the decomposition of the original Ag NC intermediates to thiolate–Ag^I complexes by the excess GSH ligands in water. Step C—the reduction of the type-II complexes to form Ag NCs (hereafter referred to as-modified Ag NC intermediates). The addition of the same amount of $NaBH_4$ as that used in Step A to the type-II complex solution turned the colorless solution to light-brown after ~15 min, indicating the formation of Ag NCs in water (the modified Ag NC intermediates). The modified Ag NC intermediates were then incubated in water at room temperature for 8 h (Stage II in Scheme 1), and a strong red emission in water was observed under UV illumination at 365 nm, implicating the formation of strongly r-Ag NCs.

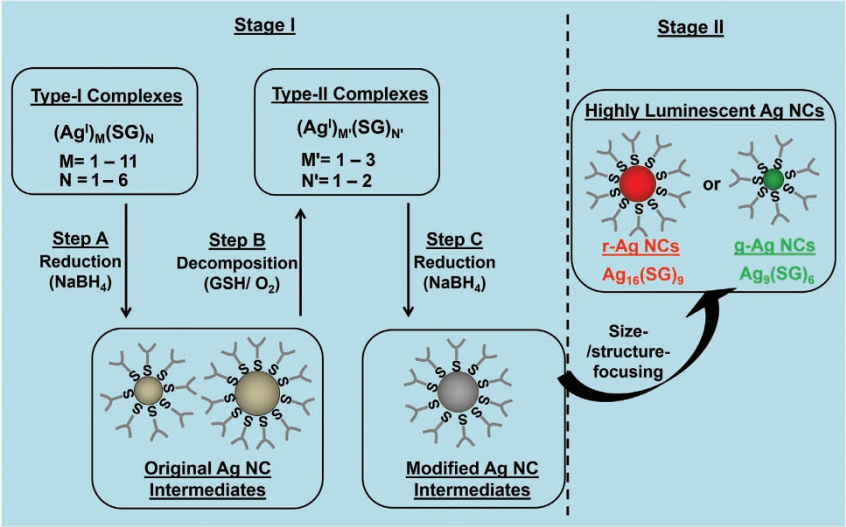

Scheme 1 Schematic illustration of the process to generate highly luminescent GSH-protected Ag NCs in water.

The key strategy in our protocol was to modify Ag NC intermediates in water that were subjected to a final size-/structure-focusing process to generate highly luminescent Ag NCs. It has been well-demonstrated in the synthesis of Au NCs that the size and structure properties of the Au NC intermediates that are subjected to a further size-/structure-focusing are crucial to produce Au NCs with a well-defined size and structure.[54–59] We reasoned that this principle was also applicable in the synthesis of thiol-protected Ag NCs. The optical properties and size/structure information of the type-I and type-II complexes and those of the original and modified Ag NC intermediates have been characterized by UV–vis spectroscopy and electrospray ionization (ESI) or matrix-assisted laser desorption ionization time-of-flight (MALDI-TOF) mass spectrometry.

Characterization of the thiolate–Ag^I complexes and Ag NC intermediates

As shown in Figure 1a, although both type-I and type-II complexes were colorless in water (inset, item no. 1 and no. 3), they showed very different optical absorption spectra: the type-I complexes displayed two distinct absorption peaks at 280 and 370 nm (Figure 1a, curve no. 1), whereas the type-II complexes did not show any obvious absorption peak in the 300–900 nm region (curve no. 3). The peak at 370 nm in the absorption spectrum of type-I complexes was associated with the metallophilic interaction between the metal centers ($Ag^I \cdots Ag^I$), which is well-documented for closed-shell metal atoms (Ag^I has $4d^{10}$ center).[60–62] The formation of metallophilic bonds between the thiolate–Ag^I complexes implied that there was a certain extent of intermolecular aggregations in the type-I complexes, as confirmed by its ESI mass spectrum. As shown in Figure 1b (top panel), the species in the type-I thiolate–Ag^I complexes displayed a very broad size range from Ag_1 *to* Ag_{11} (or $Ag_{1–11}$ species, see Supplementary Figure S1 for their detailed isotope patterns). On the contrary, the ESI mass spectrum of the type-II complexes (Figure 1b, bottom panel) only showed small complex species with a very narrow size range from Ag_1 *to* Ag_3 ($Ag_{1–3}$), which was also consistent with the observation of no obvious absorption peaks in its absorption spectrum (Figure 1a, curve no. 3). It should be mentioned that a cycle of the reduction–decomposition process was indispensable for the formation of type-II complexes with a narrower size range. As evidence, a long incubation time (for example, 24 h) of the type-I complexes did not confine their size range, which was indicated by their unchanged optical absorption spectrum (data not shown). This finding excludes the possibility that the type-II complexes were the thermodynamic product of the type-I complexes after a long incubation time. In addition, the characterization of these two complexes by transmission electron microscopy (TEM) was not successful owing to their excessively unconsolidated composition. On the other hand, there was no difference in the binding energy of Ag $3d_{5/2}$ in type-I and type-II thiolate–Ag^I complexes (see X-ray photoelectron spectroscopy analyses in Supplementary Figure S2), which provided supporting evidence of the unchanged oxidation states of Ag in the complexes before (type-I) and after a reduction–decomposition modification (type-II). Nevertheless, compared with the type-I thiolate–Ag^I complexes, the relatively narrower size distribution and smaller species in type-II complexes favored the subsequent formation of Ag NCs (upon the reduction) with improved controllability of size and structure.

The introduction of the same amount of a strong reducing agent, $NaBH_4$, into the type-I and type-II thiolate–Ag^I complexes changed the colorless solution to a dark-red (Figure 1a inset, item no. 2) and light-brown (item no.4) solution, respectively, indicating the formation of Ag NCs in water. These two Ag NCs also displayed apparent distinctions in water. The original Ag NC intermediates (from the reduction of type-I complexes) showed a distinct absorption peak at 480 nm and three shoulder peaks at 335, 540 and 645 nm (Figure 1a, curve no.2), while the shoulder peak at 540 nm disappeared for the modified Ag NC intermediates (curve no.4). The different optical absorption spectra of these two Ag NC intermediates indicated that they could have different cluster sizes and/or structures. TEM images showed that the size of both the original and modified Ag NC intermediates was below 2 nm (Supplementary Figure S3). MALDI-TOF mass spectrometry was used to further examine the cluster size of the original and modified Ag NC intermediates. As shown in Figure 1c, the original Ag NC intermediates (top panel) showed a broad band from 2180 to 5725 Da in the mass spectrum, implying that the original Ag NC intermediates possessed a polydispersed size nature, mainly from Ag_6 *to* Ag_{19} ($Ag_{6–19}$ NCs). On the contrary, the modified Ag NC intermediates possessed a relatively narrower size

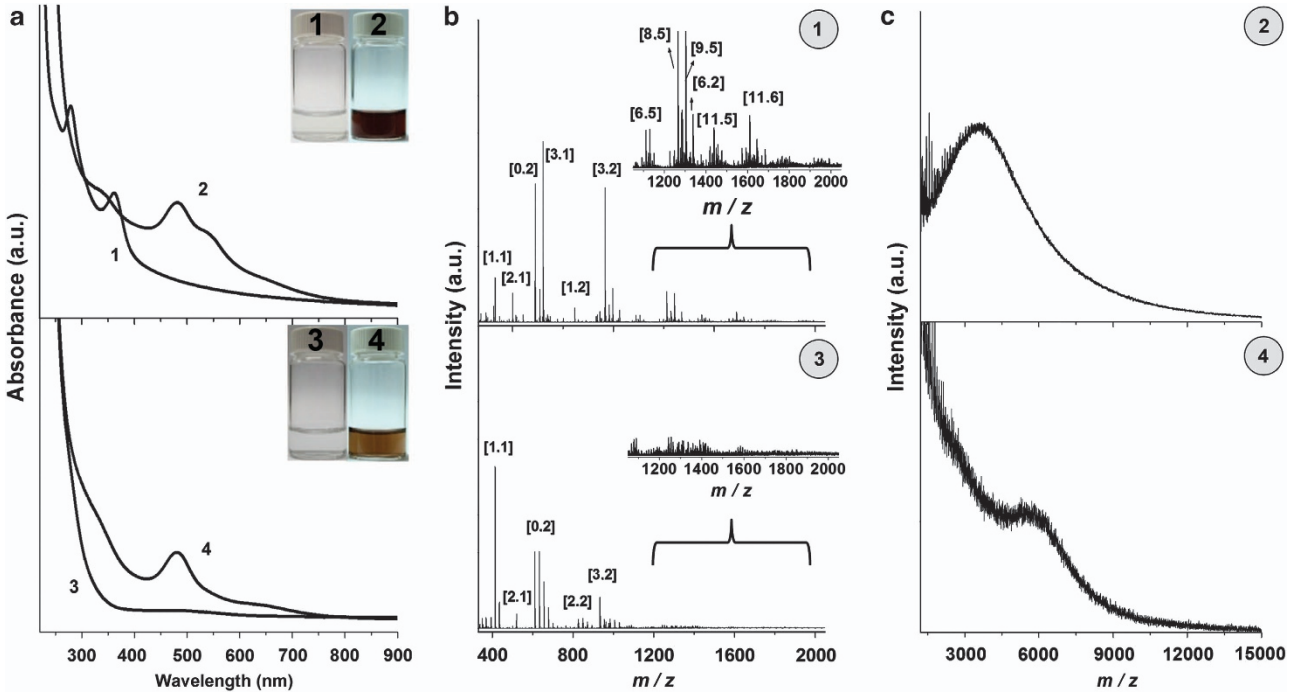

Figure 1 (**a**) Optical absorption spectra and photographs (inset) of the type-I (no. 1) and type-II (no. 3) complexes and the original (no. 2) and modified (no. 4) Ag NC intermediates. (**b**) ESI mass spectra of the type-I (top, no. 1) and type-II (bottom, no. 3) complexes. The inset shows the zoomed-in ESI mass spectra of the complexes in a *m*/*z* range of 1050–2050. (**c**) MALDI-TOF mass spectra of the original (top, no. 2) and modified (bottom, no. 4) Ag NC intermediates.

distribution from 5310 to 6140 Da (Figure 1c, bottom panel), which could be assigned to $Ag_{18}(SG)_{11}$ *to* $Ag_{20}(SG)_{13}$. The difference in cluster size between the two Ag NC intermediates was also suggested by their different formation rate. The reduction of type-I thiolate–Ag^I complexes to form Ag NCs (the original Ag NC intermediates) was completed within 5 min. However, ~15 min was needed to form the modified Ag NC intermediates upon the addition of $NaBH_4$ to the type-II thiolate–Ag^I complexes. The different reduction kinetics of the two types of complexes upon the introduction of the strong reducing agent could be understood from their distinct size and structure differences. The smaller and more monodispersed complex species (the type-II complexes) were more thermodynamically stable and more resistant to the reducing agent, thus slowing down the reduction kinetics and generating NCs (the modified Ag NC intermediates) with better definitive size and possibly a more compact structure.

Synthesis and characterization of r-Ag NCs

No luminescence was emitted by the original or modified Ag NC intermediates in aqueous solution (Supplementary Figure S4). The original Ag NC intermediates were very vulnerable to the excess thiol ligands in water and completely decomposed into thiolate–Ag^I complexes within 3 h. On the contrary, the modified Ag NC intermediates exhibited much better stability against the excess thiol ligands in water, possibly because of their more compact structure and narrower size distribution ($Ag_{18}(SG)_{11}$ *to* $Ag_{20}(SG)_{13}$). The more robust Ag NC intermediates therefore created a better-controlled size-/structure-focusing process in water, which favored the formation of stable Ag NCs with a well-defined structure. Other metastable NC species were gradually decomposed by this size-/structure-focusing process. As a result, a very strong red emission (inset of Figure 2a) was observed after 8 h of incubation of the modified Ag NC intermediates at room temperature. It should be mentioned that further incubation (for example, to 48 h) of the reaction solution had a negligible effect on the fluorescence intensity. The strong luminescence observed in aqueous solution was most likely emitted by the stable Ag NCs with a well-defined structure. The emission peak of the as-synthesized r-Ag NCs was 647 nm (Figure 2a, red line) with an excitation of 489 nm. The quantum yield was ~4.2% (calibrated with Rhodamine B). It was observed that the shoulder absorption peaks at 335 and 645 nm of the modified Ag NC intermediates (Figure 1a, curve no.4) disappeared after 8 h of incubation, and the absorption peak at 480 nm became much sharper and slightly shifted to 489 nm (Figure 2a, black line), indicating size/structure focusing of the modified Ag NC intermediates in water occurred owing to the etching of metastable Ag NC species.

Strongly red-emitting Ag NCs with a well-defined size and structure were formed after the size-/structure-focusing process, which was confirmed by MALDI-TOF and ESI mass spectrometric analysis. In the MALDI-TOF spectrum (Figure 2b), a peak at ~4485 Da was detected, which agrees well with the molecular formula of $Ag_{16}(SG)_9$. ESI mass spectroscopy was also used to verify the cluster formula. As shown in Figure 2c (top panel), four sets of intense peaks at m/z of 1516, 1629, 1735 and 1946 were present in the m/z range of 1400–3000, which could be attributed to $[Ag_{16}(SG)_9]^{3-}$, $[Ag_{12}(SG)_6]^{2-}$, $[Ag_{16}(SG)_{11}]^{3-}$, and $[Ag_{16}(SG)_7]^{2-}$, respectively. Therefore, the as-synthesized r-Ag NCs can be assigned to $Ag_{16}(SG)_9$ on the basis of its MALDI-TOF and ESI mass spectra. The other species observed in the ESI mass spectrum could be generated either by the fragmentation or the rearrangement/recombination of Ag NCs during ionization. Similar observations have been reported in previous publications.[58,63] TEM images (Supplementary Figure S5) also confirmed that the sizes of the r-Ag NCs were below 1.5 nm. The r-Ag NCs, with a formula of $Ag_{16}(SG)_9$, are a new species in the family of thiol-protected Ag NCs. The r-Ag NCs have shown excellent

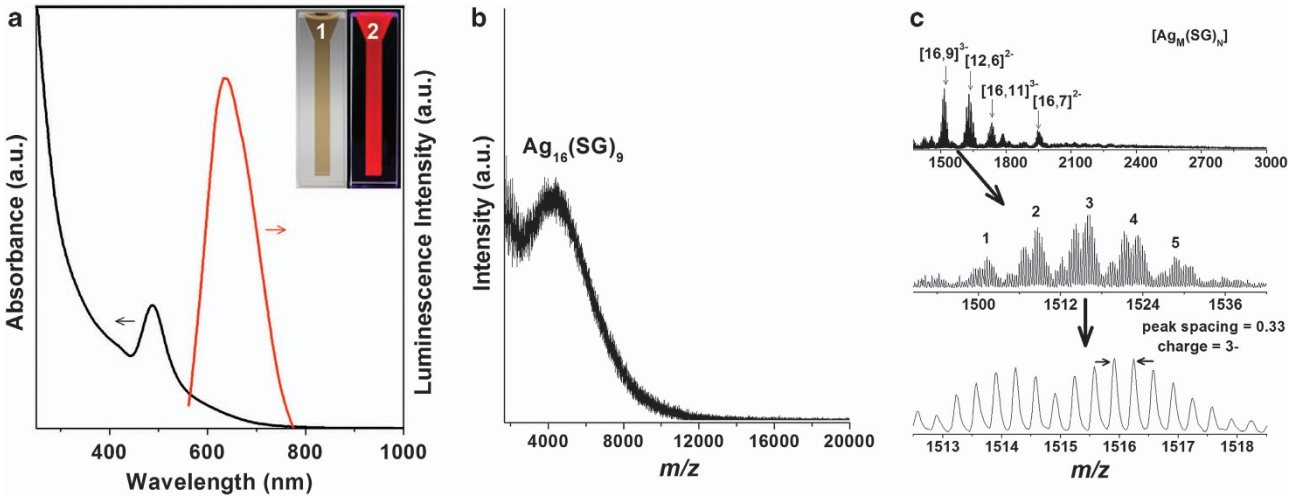

Figure 2 (**a**) Optical absorption (black line) and photoemission (red line, $\lambda_{ex} = 489$ nm) spectra of r-Ag NCs in water. The inset shows photographs of r-Ag NCs in water under visible (item 1) and UV (item 2) light. (**b**) MALDI-TOF mass spectrum of r-Ag NCs in water. (**c**) ESI mass spectra (in negative ion mode) of r-Ag NCs: the broad-range spectrum of $Ag_M(SG)_N$ (top), the zoomed-in spectrum of the species of $[Ag_{16}(SG)_9 - 5H + 3Na]^{3-}$ (middle) and the isotope pattern of $[Ag_{16}(SG)_9 - 5H + 3Na]^{3-}$ (bottom; the observed mass of 4547.7 Da, and the calculated mass of 4546.8 Da).

stability in water. The luminescence loss was very low at less than 10% even after 3 months of storage at 4 °C (Supplementary Figure S6a). It is believed that after a size-/structure-focusing process, the metastable NC species in water gradually decomposed, leaving behind the most stable Ag NCs with a well-defined size and structure, which could also be considered magic-size Ag NCs. Recent studies have shown that thiol-protected magic-size Au NCs are extraordinarily stable because of the electron-shell closure.[64,65] The same magic-size theory could also apply to the thiol-protected Ag NCs. The r-Ag NCs carry one negative charge, $[Ag_{16}(SG)_9]^-$, and have 8 valence electrons in each cluster ($16-9+1=8e$, assuming each thiol ligand withdraws one electron due to the Ag-S bond formation), corresponding to one of the most common shell-closing structures according to the 'superatom electronic theory'.[66,67] This ultrastable magic-size Ag NC species possessed a well-defined size and structure and could emit strong luminescence. However, it should be stated that a more precise description of the luminescence property of r-Ag NCs has to await the results of total structure determination based on X-ray crystallographic analysis of single crystals of the Ag NCs, which is still a significant challenge in current NC research.

Several experimental observations have helped to determine the origin of the luminescence of our sample (r-Ag NCs): 1) there was no luminescence in the system without the presence of $AgNO_3$ (for example, only GSH, $NaBH_4$ and their mixtures), suggesting that the red emission in our product was due to Ag NCs; 2) the luminescence was unlikely to be produced by small thiolate-Ag^I complexes, as materials with a molecular weight <3000 Da had been removed using a filter with a 3000-Da molecular weight cut-off (MWCO). As shown in Supplementary Figure S7, an almost identical emission spectrum of the filtered product has been observed for the raw product, suggesting that the luminescence was emitted from Ag NCs in our sample; and 3) only one distinct band was observed in the native polyacrylamide gel electrophoresis (PAGE) analysis of the as-synthesized r-Ag NCs (Supplementary Figure S8, inset, item 1). This band also showed strong red emission under UV light (item 2). In addition, the isolated luminescent species from the native PAGE gel showed similar absorption (Supplementary Figure S8, black line) and emission (red line) spectra as those of raw r-Ag NCs (Figure 2a), further confirming that the luminescence was generated by the Ag NCs in our sample.

Synthesis and characterization of g-Ag NCs

Another noticeable feature of our protocol was color tunability. It is well-known that metal NCs possess size-tunable electronic transitions and exhibit a size-dependent luminescence property.[65] The emission color of our final products can be adjusted by simply fine-tuning the size of the modified Ag NC intermediates. One feasible approach to adjust the size of the modified Ag NC intermediates is to introduce different concentrations of the reducing agent ($NaBH_4$) in the type-II thiolate-Ag^I complex solution. This adjustment of reduction kinetics led to the formation of Ag NC intermediates with various sizes. For instance, the addition of more reducing agent $NaBH_4$ (250 μl vs 50 μl that was used in the synthesis of r-Ag NCs) can increase the reduction rate of the type-II complexes, therefore producing Ag NCs (the modified Ag NC intermediates) with smaller size. As shown in Supplementary Figure S9, the as-modified Ag NC intermediates displayed a light-brown color in solution and exhibited two absorption peaks at 420 and 520 nm. A representative TEM image of the modified Ag NC intermediates confirmed that they were less than 2 nm in size (Supplementary Figure S10). The MALDI-TOF mass spectrum of the modified Ag NC intermediates displayed a prominent peak at ~3960 Da (Supplementary Figure S11), which was indeed much smaller, as expected, than the size of the modified Ag NC intermediates prepared with 50 μl of $NaBH_4$ (~6000 Da, Figure 1c, bottom panel).

Similar to the formation of r-Ag NCs, the incubation of the as-modified Ag NC intermediates for 48 h at room temperature produced strongly g-Ag NCs in water (inset of Figure 3a). As shown in Figure 3a, the g-Ag NCs displayed an emission peak at 495 nm (blue line). The quantum yield of the g-Ag NCs was determined to be ~2.6% by calibrating with Rhodamine B. The absorption peaks of the modified Ag NC intermediates at 420 and 520 nm (Supplementary Figure S9) disappeared after 48 h of incubation, and a new shoulder peak at 370 nm was observed for the g-Ag NCs (Figure 3a, black line). Both MALDI-TOF and ESI mass spectra suggested that $Ag_9(SG)_6$ was the dominant species in the g-Ag NCs

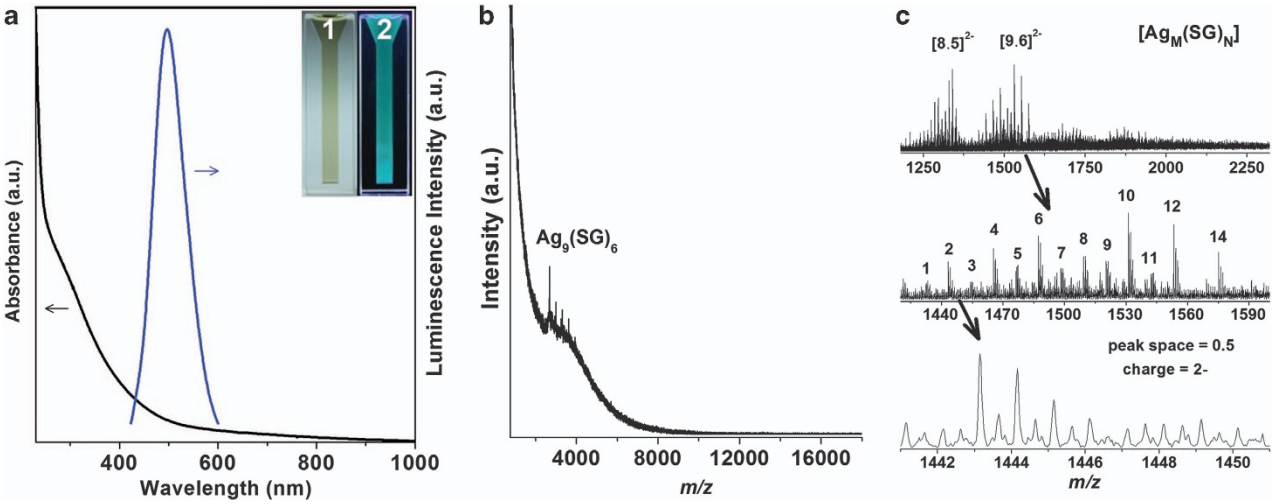

Figure 3 (**a**) Optical absorption (black line) and photoemission (blue line, $\lambda_{ex} = 379$ nm) spectra of g-Ag NCs in water. The inset shows photographs of g-Ag NCs in water under visible (item 1) and UV (item 2) light. (**b**) MALDI-TOF mass spectrum of g-Ag NCs in water. (**c**) ESI mass spectra (in negative ion mode) of g-Ag NCs: the broad-range spectrum of $Ag_M(SG)_N$ (top), the zoomed-in spectrum of the species of $[Ag_9(SG)_6 - 5H + 2Na + K]^{2-}$ (middle) and the isotope pattern of $[Ag_9(SG)_6 - 5H + 2Na + K]^{2-}$(bottom; the observed mass of 2888.3 Da, and the calculated mass of 2888.7 Da).

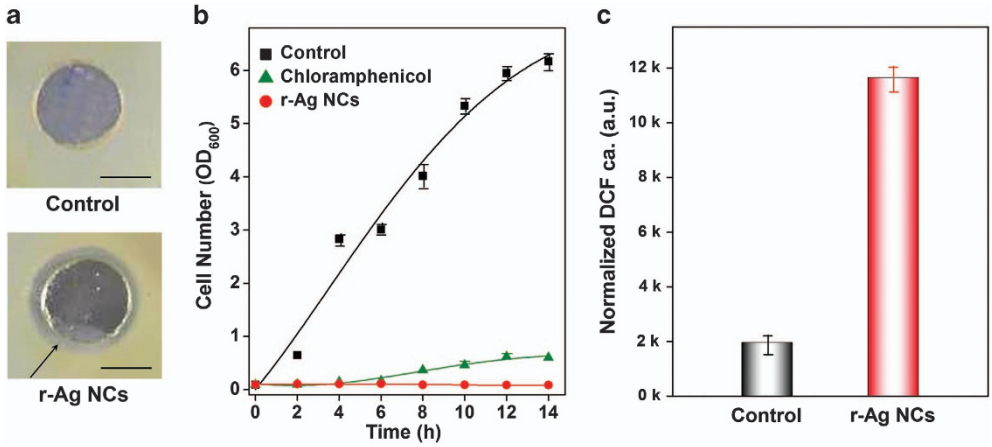

Figure 4 (**a**) Agar diffusion assay showing the presence of a clear zone surrounding the well where r-Ag NCs were introduced (scale bar of 1 cm). (**b**) Comparison in cell numbers between the control sample, the sample with chloramphenicol and the sample with r-Ag NCs during a period of 14 h incubation. (**c**) Comparison of the ROS concentration of cells between the control sample and the r-Ag NCs sample.

(Figures 3b and c). The $Ag_8(SG)_5$ presented in the ESI spectrum could have been the residue of the parent $Ag_9(SG)_6$ clusters after the common dissociation of an Ag(SG) fragment. The TEM image (Supplementary Figure S5b) showed that the g-Ag NCs were < 1.5 nm in size. The g-Ag NCs, with a molecular formula of $Ag_9(SG)_6$, were smaller than the r-Ag NCs, with a formula of $Ag_{16}(SG)_9$, which corresponds well with their size-dependent luminescence property—the wavelength shift from red (647 nm) for r-Ag NCs to green (495 nm) for g-Ag NCs, with a decrease in the cluster size from Ag_{16} to Ag_9. Similar to r-Ag NCs, the as-synthesized g-Ag NCs also showed good stability in water (Supplementary Figure S6b). Using our novel principle of aqueous-based synthesis of luminescent thiol-protected Ag NCs, it is possible to synthesize luminescent Ag NCs with distinct characteristics and to equip the bioimaging toolkit with a rainbow (from blue to near-infrared) of Ag NCs.

Superior antimicrobial activity of the Ag NCs

The ultrafine size of the as-synthesized Ag NCs may provide an additional feature, namely, superior antimicrobial activity owing to their ultra-high surface to volume ratio and unique surface chemistry compared with their larger counterparts (nanocrystals with size > 2 nm). *P. aeruginosa* was chosen as a bacterial model to study the antimicrobial properties of the r-Ag NCs. *P. aeruginosa* has been reported to cause pneumonia,[68] urinary tract infections[68,69] and respiratory system infections in many burn cases[70] and immune-suppressed AIDS patients.[68,71] Recent reports also showed an increased amount of *P. aeruginosa* resistance towards many conventional antibiotics, such as ampicillin, penicillin and cephalosporin.[24,68] The susceptibility of *P. aeruginosa* towards r-Ag NCs was first determined by an agar diffusion assay. Our results confirmed that as little as 8 μg of r-Ag NCs can effectively inhibit the growth of *P. aeruginosa*. This result was shown by the clear zone, with a width of ~3.9 mm, surrounding the wells in which the Ag NC suspension was introduced (Figure 4a, indicated by the arrow).

To further affirm the efficacy of the r-Ag NCs against *P. aeruginosa*, we treated *P. aeruginosa* culture with 500 μM (on the basis of Ag atoms) of an r-Ag NC suspension and observed the cell growth over a time course of 14 h (Figure 4b). Our results showed that at

concentration of 500 μM, Ag NCs completely inhibited *P. aeruginosa* growth with no significant increase in culture density turbidity (Figure 4b, red line). The inhibition effect was comparable with that of chloramphenicol used at the same concentration (Figure 4b, green line). We also observed that at lower concentration (45 μM), r-Ag NCs prolonged the *P. aeruginosa* lag phase and retarded its growth until 8 h of incubation. However, after 24 h of incubation, the growth inhibitory effect of the r-Ag NCs had significantly diminished (data not shown). This observation leads us to believe that there is an optimum working concentration of the newly developed r-Ag NCs to effectively inhibit the growth of and/or kill pathogenic bacteria. Thus, we proceeded to determine the minimum inhibitory concentration (MIC) and minimum bactericidal concentration (MBC) of r-Ag NCs.

As shown in Supplementary Figure S12, similar to many other antimicrobial agents, the r-Ag NCs showed dose-dependent bactericidal properties. The MIC and MBC correspond to the concentration that inhibited bacterial growth as much as 90% and 99.9%, respectively, compared with the vehicle control. Our results showed that the MIC and MBC of r-Ag NCs were 110 μM ($\sim$11.8 mg l^{-1}) and 230 μM ($\sim$24.6 mg l^{-1}), respectively. These values are much lower than those of commercially available Ag nanocrystals, which are reported to have an MIC of 83.3 mM ($\sim$9000 mg l^{-1}) and an MBC of 100 mM ($\sim$10 000 mg l^{-1}).[72] We believe that the main reason for the lower MIC and MBC values reported in our study is owing to the smaller size of our r-Ag NCs ($<$1.5 nm) compared with those used in the previous publication ($\sim$100 nm).[72] These high-potency Ag NC antimicrobial capabilities could significantly reduce the possible side effects of Ag antimicrobials because a much lower dosage than that of larger Ag nanocrystals is needed to acquire similar antimicrobial activity.[73–75]

To understand the underlying mechanism of the antimicrobial ability of our Ag NCs, we measured the level of the intracellular ROS in the *P. aeruginosa* population after exposure to r-Ag NCs. Our observation showed that there was approximately a sixfold increase in the oxidized DCF concentration (Figure 4c). This confirmed that r-Ag NCs could generate ROS to eliminate pathogenic bacteria, similar to two earlier observations using Ag nanocrystals.[25,76] Nevertheless, an added advantage of our Ag NCs is their strong red luminescence, which can be further used to develop a real-time monitoring system for the antimicrobial process, shedding light on the working mechanism of Ag antimicrobials and providing useful information for the design of more efficient Ag antimicrobials.

CONCLUSION

In summary, we have developed a simple and facile synthesis strategy for water-soluble thiol-protected Ag NCs with strong luminescence and tunable emissions. A new cyclic process of reduction–decomposition–reduction was applied to suitably modify the Ag NC intermediates, making a subsequent size-/structure-focusing process in a well-controlled environment possible and thus generating highly luminescent Ag NCs with a well-defined size and structure. Strong r- and g-Ag NCs were synthesized with molecular formulae of $Ag_{16}(SG)_9$ and $Ag_9(SG)_6$, respectively. The as-synthesized r- and g-Ag NCs were protected by a natural tripeptide (GSH) and exhibited excellent stability in water, which could facilitate their potential biomedical applications. The protocols and products developed in this study are important not only because they provide a simple, versatile, efficient and 'green' method for the production of highly luminescent Ag NCs but also because they exemplify the importance of the size/structure features of the Ag NC intermediates subjected to a final focusing process, which can be used towards the future synthesis of luminescent Ag NCs covering the visible spectrum (blue to near-infrared). We have also shown that our r-Ag NCs possessed superior bactericidal properties against *P. aeruginosa*. These ultrafine luminescent Ag NCs could be further developed as a new high-efficiency antimicrobial agent.

CONFLICT OF INTEREST

The authors declare no conflict of interest.

ACKNOWLEDGEMENTS

We thank Professor Ting Yen Peng (Department of Chemical and Biomolecular Engineering, NUS) for his kind gift of the *P. aeruginosa* strain. This work is financially supported by the Ministry of Education, Singapore, under Grants R-279-000-295-133, R-279-000-327-112 and R-279-000-350-112. X Yuan acknowledges the National University of Singapore for his research scholarship.

1 Jin, R. C. Quantum sized, thiolate-protected gold nanoclusters. *Nanoscale* **2,** 343–362 (2010).
2 Diez, I. & Ras, R. H. A. Fluorescent silver nanoclusters. *Nanoscale* **3,** 1963–1970 (2011).
3 Zhang, Q. B., Xie, J. P., Yu, Y. & Lee, J. Y. Monodispersity control in the synthesis of monometallic and bimetallic quasi-spherical gold and silver nanoparticles. *Nanoscale* **2,** 1962–1975 (2010).
4 Shang, L., Dong, S. & Nienhaus, G. U. Ultra-small fluorescent metal nanoclusters: synthesis and biological applications. *Nano Today* **6,** 401–418 (2011).
5 Laaksonen, T., Ruiz, V., Liljeroth, P. & Quinn, B. M. Quantised charging of monolayer-protected nanoparticles. *Chem. Soc. Rev.* **37,** 1836–1846 (2008).
6 González, B. S., Rodriáguez, M. A. J., Blanco, C., Rivas, J., Loápez-Quintela, M. A. & Martinho, J. M. G. One step synthesis of the smallest photoluminescent and paramagnetic PVP-protected gold atomic clusters. *Nano Lett.* **10,** 4217–4221 (2010).
7 Xie, J. P., Zheng, Y. G. & Ying, J. Y. Protein-directed synthesis of highly fluorescent gold nanoclusters. *J. Am. Chem. Soc.* **131,** 888–889 (2009).
8 Xu, H. & Suslick, K. S. Water-soluble fluorescent silver nanoclusters. *Adv. Mater.* **22,** 1078–1082 (2010).
9 Choi, S., Dickson, R. M. & Yu, J. Developing luminescent silver nanodots for biological applications. *Chem. Soc. Rev.* **41,** 1867–1891 (2012).
10 Tanaka, S.-I., Miyazaki, J., Tiwari, D. K., Jin, T. & Inouye, Y. Fluorescent platinum nanoclusters: synthesis, purification, characterization, and application to bioimaging. *Angew. Chem. Int. Ed.* **50,** 431–435 (2011).
11 Wei, W., Lu, Y., Chen, W. & Chen, S. One-pot synthesis, photoluminescence, and electrocatalytic properties of subnanometer-sized copper clusters. *J. Am. Chem. Soc.* **133,** 2060–2063 (2011).
12 Yu, J., Patel, S. A. & Dickson, R. M. *In vitro* and intracellular production of peptide-encapsulated fluorescent silver nanoclusters. *Angew. Chem. Int. Ed.* **46,** 2028–2030 (2007).
13 Zhou, C., Long, M., Qin, Y., Sun, X. & Zheng, J. Luminescent gold nanoparticles with efficient renal clearance. *Angew. Chem. Int. Ed.* **50,** 3168–3172 (2011).
14 Resch-Genger, U., Grabolle, M., Cavaliere-Jaricot, S., Nitschke, R. & Nann, T. Quantum dots versus organic dyes as fluorescent labels. *Nat. Meth.* **5,** 763–775 (2008).
15 Bottrill, M. & Green, M. Some aspects of quantum dot toxicity. *Chem. Commun.* **47,** 7039–7050 (2011).
16 Shang, L., Azadfar, N., Stockmar, F., Send, W., Trouillet, V., Bruns, M., Gerthsen, D. & Nienhaus, G. U. One-pot synthesis of near-infrared fluorescent gold clusters for cellular fluorescence lifetime imaging. *Small* **7,** 2614–2620 (2011).
17 Yeh, H.-C., Sharma, J., Han, J. J., Martinez, J. S. & Werner, J. H. A DNA-silver nanocluster probe that fluoresces upon hybridization. *Nano Lett.* **10,** 3106–3110 (2010).
18 Guo, W., Yuan, J., Dong, Q. & Wang, E. Highly sequence-dependent formation of fluorescent silver nanoclusters in hybridized DNA duplexes for single nucleotide mutation identification. *J. Am. Chem. Soc.* **132,** 932–934 (2009).
19 Yang, S. W. & Vosch, T. Rapid detection of microrna by a silver nanocluster DNA probe. *Anal. Chem.* **83,** 6935–6939 (2011).
20 Yu, J., Choi, S. & Dickson, R. M. Shuttle-based fluorogenic silver-cluster biolabels. *Angew. Chem. Int. Ed.* **48,** 318–320 (2009).
21 Lu, Y. & Chen, W. Sub-nanometre sized metal clusters: from synthetic challenges to the unique property discoveries. *Chem. Soc. Rev.* **41,** 3594–3623 (2012).
22 Project on Emerging Nanotechnologies. Silver Nanotechnology: A database of silver nanotechnology in commercial products (2011).
23 Chen, M. W., Yang, Z. W., Wu, H. M., Pan, X., Xie, X. B. & Wu, C. B. Antimicrobial activity and the mechanism of silver nanoparticle thermosensitive gel. *Int. J. Nanomed.* **6,** 2873–2877 (2011).
24 Fisher, J. F., Meroueh, S. O. & Mobashery, S. Bacterial resistance to β-lactam antibiotics: compelling opportunism, compelling opportunity. *Chem. Rev.* **105,** 395–424 (2005).

25 Kim, J. S., Kuk, E., Yu, K. N., Kim, J. H., Park, S. J., Lee, H. J., Kim, S. H., Park, Y. K., Park, Y. H., Hwang, C. Y., Kim, Y. K., Lee, Y. S., Jeong, D. H. & Cho, M. H. Antimicrobial effects of silver nanoparticles. *Nanomed. Nanotechnol.* **3,** 95–101 (2007).
26 Morones, J. R., Elechiguerra, J. L., Camacho, A., Holt, K., Kouri, J. B., Ramirez, J. T. & Yacaman, M. J. The bactericidal effect of silver nanoparticles. *Nanotechnology* **16,** 2346–2353 (2005).
27 Maity, D., Kanti Bain, M., Bhowmick, B., Sarkar, J., Saha, S., Acharya, K., Chakraborty, M. & Chattopadhyay, D. *In situ* synthesis, characterization, and antimicrobial activity of silver nanoparticles using water soluble polymer. *J. Appl. Polym. Sci.* **122,** 2189–2196 (2011).
28 Pal, S., Tak, Y. K. & Song, J. M. Does the antibacterial activity of silver nanoparticles depend on the shape of the nanoparticle? A study of the gram-negative bacterium *Escherichia coli*. *Appl. Environ. Microbiol.* **73,** 1712–1720 (2007).
29 Shahverdi, A. R., Fakhimi, A., Shahverdi, H. R. & Minaian, S. Synthesis and effect of silver nanoparticles on the antibacterial activity of different antibiotics against *Staphylococcus aureus* and *Escherichia coli*. *Nanomed.: Nanotechnol.* **3,** 168–171 (2007).
30 Martínez-Castañón, G., Niño-Martínez, N., Martínez-Gutierrez, F., Martínez-Mendoza, J. & Ruiz, F. Synthesis and antibacterial activity of silver nanoparticles with different sizes. *J. Nanopart. Res.* **10,** 1343–1348 (2008).
31 Wu, Z., Wang, M., Yang, J., Zheng, X., Cai, W., Meng, G., Qian, H., Wang, H. & Jin, R. Well-defined nanoclusters as fluorescent nanosensors: a case study on $Au_{25}(SG)_{18}$. *Small* **8,** 2028–2035 (2012).
32 Duan, H. & Nie, S. Etching colloidal gold nanocrystals with hyperbranched and multivalent polymers: a new route to fluorescent and water-soluble atomic clusters. *J. Am. Chem. Soc.* **129,** 2412–2413 (2007).
33 Lin, C. A. J., Yang, T. Y., Lee, C. H., Huang, S. H., Sperling, R. A., Zanella, M., Li, J. K., Shen, J. L., Wang, H. H., Yeh, H. I., Parak, W. J. & Chang, W. H. Synthesis, characterization, and bioconjugation of fluorescent gold nanoclusters toward biological labeling applications. *ACS Nano* **3,** 395–401 (2009).
34 Liu, Y. L., Ai, K. L., Cheng, X. L., Huo, L. H. & Lu, L. H. Gold-nanocluster-based fluorescent sensors for highly sensitive and selective detection of cyanide in water. *Adv. Funct. Mater.* **20,** 951–956 (2010).
35 Huang, C. -C., Yang, Z., Lee, K.-H. & Chang, H.-T. Synthesis of highly fluorescent gold nanoparticles for sensing mercury(II). *Angew. Chem. Int. Ed.* **46,** 6824–6828 (2007).
36 Luo, Z., Yuan, X., Yu, Y., Zhang, Q., Leong, D. T., Lee, J. Y. & Xie, J. From aggregation-induced emission of Au(I)–thiolate complexes to ultrabright Au(0)@Au(I)–thiolate core–shell nanoclusters. *J. Am. Chem. Soc.* **134,** 16662–16670 (2012).
37 Xu, H. X. & Suslick, K. S. Sonochemical synthesis of highly fluorescent Ag nanoclusters. *ACS Nano* **4,** 3209–3214 (2010).
38 Shen, Z., Duan, H. & Frey, H. Water-soluble fluorescent Ag nanoclusters obtained from multiarm star poly(acrylic acid) as "molecular hydrogel" templates. *Adv. Mater.* **19,** 349–352 (2007).
39 Shang, L. & Dong, S. J. Facile preparation of water-soluble fluorescent silver nanoclusters using a polyelectrolyte template. *Chem. Commun.* 1088–1090 (2008).
40 Zheng, J. & Dickson, R. M. Individual water-soluble dendrimer-encapsulated silver nanodot fluorescence. *J. Am. Chem. Soc.* **124,** 13982–13983 (2002).
41 Petty, J. T., Zheng, J., Hud, N. V. & Dickson, R. M. DNA-templated Ag nanocluster formation. *J. Am. Chem. Soc.* **126,** 5207–5212 (2004).
42 Richards, C. I., Choi, S., Hsiang, J.-C., Antoku, Y., Vosch, T., Bongiorno, A., Tzeng, Y.-L. & Dickson, R. M. Oligonucleotide-stabilized Ag nanocluster fluorophores. *J. Am. Chem. Soc.* **130,** 5038–5039 (2008).
43 Gwinn, E. G., O'Neill, P., Guerrero, A. J., Bouwmeester, D. & Fygenson, D. K. Sequence-dependent fluorescence of DNA-hosted silver nanoclusters. *Adv. Mater.* **20,** 279–283 (2008).
44 Narayanan, S. S. & Pal, S. K. Structural and functional characterization of luminescent silver-protein nanobioconjugates. *J. Phys. Chem. C* **112,** 4874–4879 (2008).
45 Guo, C. & Irudayaraj, J. Fluorescent Ag clusters via a protein-directed approach as a Hg(II) ion sensor. *Anal. Chem.* **83,** 2883–2889 (2011).
46 Bakr, O. M., Amendola, V., Aikens, C. M., Wenseleers, W., Li, R., Dal Negro, L., Schatz, G. C. & Stellacci, F. Silver nanoparticles with broad multiband linear optical absorption. *Angew. Chem. Int. Ed.* **48,** 5921–5926 (2009).
47 Udaya Bhaskara Rao, T. & Pradeep, T. Luminescent Ag_7 and Ag_8 clusters by interfacial synthesis. *Angew. Chem. Int. Ed.* **49,** 3925–3929 (2010).
48 Yuan, X., Luo, Z., Zhang, Q., Zhang, X., Zheng, Y., Lee, J. Y. & Xie, J. Synthesis of highly fluorescent metal (Ag, Au, Pt, and Cu) nanoclusters by electrostatically induced reversible phase transfer. *ACS Nano* **5,** 8800–8808 (2011).
49 Yuan, X., Yeow, T. J., Zhang, Q., Lee, J. Y. & Xie, J. Highly luminescent Ag^+ nanoclusters for Hg^{2+} ion detection. *Nanoscale* **4,** 1968–1971 (2012).
50 Wang, C., Xu, L., Wang, Y., Zhang, D., Shi, X., Dong, F., Yu, K., Lin, Q. & Yang, B. Fluorescent silver nanoclusters as effective probes for highly selective detection of mercury(II) at parts-per-billion levels. *Chem. Asian J.* **7,** 1652–1656 (2012).
51 Le Guével, X., Spies, C., Daum, N., Jung, G. & Schneider, M. Highly fluorescent silver nanoclusters stabilized by glutathione: a promising fluorescent label for bioimaging. *Nano Res.* **5,** 379–387 (2012).
52 Huang, S., Pfeiffer, C., Hollmann, J., Friede, S., Chen, J. J. -C., Beyer, A., Haas, B., Volz, K., Heimbrodt, W., Montenegro Martos, J. M., Chang, W. & Parak, W. J. Synthesis and characterization of colloidal fluorescent silver nanoclusters. *Langmuir* **28,** 8915–8919 (2012).
53 Dhanalakshmi, L., Udayabhaskararao, T. & Pradeep, T. Conversion of double layer charge-stabilized Ag@citrate colloids to thiol passivated luminescent quantum clusters. *Chem. Commun.* **48,** 859–861 (2012).
54 Jin, R., Qian, H., Wu, Z., Zhu, Y., Zhu, M., Mohanty, A. & Garg, N. Size focusing: a methodology for synthesizing atomically precise gold nanoclusters. *J. Phys. Chem. Lett.* **1,** 2903–2910 (2010).
55 Qian, H. & Jin, R. Ambient synthesis of $Au_{144}(SR)_{60}$ nanoclusters in methanol. *Chem. Mater.* **23,** 2209–2217 (2011).
56 Wu, Z., MacDonald, M. A., Chen, J., Zhang, P. & Jin, R. Kinetic control and thermodynamic selection in the synthesis of atomically precise gold nanoclusters. *J. Am. Chem. Soc.* **133,** 9670–9673 (2011).
57 Zhu, M., Lanni, E., Garg, N., Bier, M. E. & Jin, R. Kinetically controlled, high-yield synthesis of Au_{25} clusters. *J. Am. Chem. Soc.* **130,** 1138–1139 (2008).
58 Zhu, M., Qian, H. & Jin, R. Thiolate-protected Au_{20} clusters with a large energy gap of 2.1 ev. *J. Am. Chem. Soc.* **131,** 7220–7221 (2009).
59 Zhu, M., Qian, H. & Jin, R. Thiolate-protected $Au_{24}(SC_2H_4Ph)_{20}$ nanoclusters: superatoms or not? *J. Phys. Chem. Lett.* **1,** 1003–1007 (2010).
60 Tzeng, B. -C., Yeh, H. -T., Huang, Y. -C., Chao, H. -Y., Lee, G. -H. & Peng, S. -M. A luminescent supermolecule with gold(I) quinoline-8-thiolate: crystal structure, spectroscopic and photophysical properties. *Inorg. Chem.* **42,** 6008–6014 (2003).
61 Yu, S. -Y., Zhang, Z. -X., Cheng, E. C. -C., Li, Y. -Z., Yam, V. W. -W., Huang, H.-P. & Zhang, R. A chiral luminescent Au_{16} ring self-assembled from achiral components. *J. Am. Chem. Soc.* **127,** 17994–17995 (2005).
62 Kristiansson, O. Unusual manifestation of closed-shell interactions in silver(I) complexes: crystal structure of catena-bis(4-aminobenzoato)disilver(I) acetone solvate with ligand unsupported chains of repeated rhombohedral Ag_4 units. *Inorg. Chem.* **40,** 5058–5059 (2001).
63 Angel, L. A., Majors, L. T., Dharmaratne, A. C. & Dass, A. Ion mobility mass spectrometry of $Au_{25}(SCH_2CH_2Ph)_{18}$ nanoclusters. *ACS Nano* **4,** 4691–4700 (2010).
64 Shichibu, Y., Negishi, Y., Tsunoyama, H., Kanehara, M., Teranishi, T. & Tsukuda, T. Extremely high stability of glutathionate-protected Au_{25} clusters against core etching. *Small* **3,** 835–839 (2007).
65 Zheng, J., Nicovich, P. R. & Dickson, R. M. Highly fluorescent noble-metal quantum dots. *Annu. Rev. Phys. Chem.* **58,** 409–431 (2007).
66 Jiang, D.-e., Whetten, R. L., Luo, W. & Dai, S. The smallest thiolated gold superatom complexes. *J. Phys. Chem. C* **113,** 17291–17295 (2009).
67 Walter, M., Akola, J., Lopez-Acevedo, O., Jadzinsky, P. D., Calero, G., Ackerson, C. J., Whetten, R. L., Grönbeck, H. & Häkkinen, H. A unified view of ligand-protected gold clusters as superatom complexes. *Proc. Natl Acad. Sci. USA* **105,** 9157–9162 (2008).
68 Sacha, P., Wieczorek, P., Hauschild, T., Zorawski, M., Olszanska, D. & Tryniszewska, E. Metallo-beta-lactamases of *Pseudomonas aeruginosa*—a novel mechanism resistance to beta-lactam antibiotics. *Folia Histochem. Cytobiol.* **46,** 137–142 (2008).
69 Mittal, R., Aggarwal, S., Sharma, S., Chhibber, S. & Harjai, K. Urinary tract infections caused by *Pseudomonas aeruginosa*: a minireview. *J. Infect. Public Health* **2,** 101–111 (2009).
70 Bjarnsholt, T., Jensen, P. Ø., Fiandaca, M. J., Pedersen, J., Hansen, C. R., Andersen, C. B., Pressler, T., Givskov, M. & Høiby, N. *Pseudomonas aeruginosa* biofilms in the respiratory tract of cystic fibrosis patients. *Pediatr. Pulmonol.* **44,** 547–558 (2009).
71 Shepp, D. H., Tang, I. T. L., Ramundo, M. B. & Kaplan, M. H. Serious *Pseudomonas aeruginosa* infection in AIDS. *J. Acquir. Immune Defic. Syndr. Hum. Retrovirol.* **7,** 823–831 (1994).
72 Lara, H. H., Ayala-Nunez, N. V., Turrent, L. D. I. & Padilla, C. R. Bactericidal effect of silver nanoparticles against multidrug-resistant bacteria. *World J. Microbiol. Biotechnol.* **26,** 615–621 (2010).
73 Singh, N., Manshian, B., Jenkins, G. J. S., Griffiths, S. M., Williams, P. M., Maffeis, T. G. G., Wright, C. J. & Doak, S. H. Nanogenotoxicology: the DNA damaging potential of engineered nanomaterials. *Biomaterials* **30,** 3891–3914 (2009).
74 Kim, S., Choi, J. E., Choi, J., Chung, K. -H., Park, K., Yi, J. & Ryu, D. -Y. Oxidative stress-dependent toxicity of silver nanoparticles in human hepatoma cells. *Toxicol. In Vitro* **23,** 1076–1084 (2009).
75 Foldbjerg, R., Olesen, P., Hougaard, M., Dang, D. A., Hoffmann, H. J. & Autrup, H. PVP-coated silver nanoparticles and silver ions induce reactive oxygen species, apoptosis and necrosis in THP-1 monocytes. *Toxicol. Lett.* **190,** 156–162 (2009).
76 Park, H.-J., Kim, J. Y., Kim, J., Lee, J.-H., Hahn, J.-S., Gu, M. B. & Yoon, J. Silver-ion-mediated reactive oxygen species generation affecting bactericidal activity. *Water Res.* **43,** 1027–1032 (2009).

Supplementary Information accompanies the paper on the NPG Asia Materials website (http://www.nature.com/am)